RESEARCH ARTICLE

Flexural stiffness of feather shafts: geometry rules over material properties

Thomas Bachmann[1],*, Jens Emmerlich[2], Werner Baumgartner[3], Jochen M. Schneider[2] and
Hermann Wagner[3]

[1]Institute for Fluid Mechanics and Aerodynamics, TU Darmstadt, Petersenstr. 30, 64287 Darmstadt, Germany, [2]Materials Chemistry,
RWTH Aachen University, Kopernikusstr. 10, 52074 Aachen, Germany and [3]Institute for Biology II, RWTH Aachen University,
Mies-van-der-Rohe-Strasse 15, 52074 Aachen, Germany

*Author for correspondence (bachmann@sla.tu-darmstadt.de)

SUMMARY

Flight feathers of birds interact with the flow field during flight. They bend and twist under aerodynamic loads. Two parameters are mainly responsible for flexibility in feathers: the elastic modulus (Young's modulus, E) of the material (keratin) and the geometry of the rachises, more precisely the second moment of area (I). Two independent methods were employed to determine Young's modulus of feather rachis keratin. Moreover, the second moment of area and the bending stiffness of feather shafts from fifth primaries of barn owls (*Tyto alba*) and pigeons (*Columba livia*) were calculated. These species of birds are of comparable body mass but differ in wing size and flight style. Whether their feather material (keratin) underwent an adaptation in stiffness was previously unknown. This study shows that no significant variation in Young's modulus between the two species exists. However, differences in Young's modulus between proximal and distal feather regions were found in both species. Cross-sections of pigeon rachises were particularly well developed and rich in structural elements, exemplified by dorsal ridges and a well-pronounced transversal septum. In contrast, cross-sections of barn owl rachises were less profiled but had a higher second moment of area. Consequently, the calculated bending stiffness (EI) was higher in barn owls as well. The results show that flexural stiffness is predominantly influenced by the geometry of the feathers rather than by local material properties.

Key words: Young's modulus, feather, keratin, flexural stiffness, bending stiffness.

INTRODUCTION

Feathers of flying birds have to withstand aerodynamic forces during flight (Corning and Biewener, 1998; Usherwood et al., 2005). This holds specifically for remiges and rectrices (Berg and Rayner, 1995; Carruthers et al., 2007; Corning and Biewener, 1998). The airflow over bird wings is influenced either by active control, e.g. erection of the alula, or by passive effects such as lifting the coverts in critical flight maneuvers (Carruthers et al., 2007).

A bird's feather is composed of a central shaft and two laterally attached vanes. The shaft can be subdivided into the calamus and the rachis. The rachis is filled with a foam-like material, formed by medullary cells. This structure protects the outer region of the rachis (cortex) against buckling (Bonser, 2001). The most proximal part of the feather shaft, the calamus, anchors the feather into the bird's skin. Thereby, each calamus is supported by muscles, tendons and, in the case of remiges and rectrices, bones (Boswick and Brady, 2002; Proctor and Lynch, 1993). Vanes are formed by parallel barbs that are connected *via* hook and bow radiates. This construction results in vanes that are light, flexible and resistant to damage (Ennos et al., 1995). If a feather vane fails and splits, it can be easily reconnected by the bird with its beak. Aerodynamic forces on the vanes of flight feathers are redirected towards the skeletal elements by the rachises (Corning and Biewener, 1998). Because feathers are dead structures, their bending properties can only be influenced once – during development. Two parameters are mainly responsible for the degree of flexibility in feathers: the elastic modulus (Young's modulus, E) of the material (keratin) and its geometry, more precisely the second moment of area (I) of the rachises. A control of the dorso-ventral

bending behavior of the rachises can be achieved by an adaptation of E, I or both (Bonser and Purslow, 1995).

So far, little is known about the material properties of feather keratin. Some publications have reported the Young's modulus of feather keratin (Bonser and Purslow, 1995; Bonser, 2001; Cameron et al., 2003; Crenshaw, 1980; Fraser and Macrae, 1980; Macleod, 1980; Pannkuk et al., 2010; Purslow and Vincent, 1978), but because of different methodological approaches and species investigated, the data are hardly comparable. The few published values of Young's modulus vary between 0.045 and 10 GPa (Macleod, 1980; Purslow and Vincent, 1978).

Keratin molecules within the rachis are anisotropically arranged. This was shown in several studies. Macleod (Macleod, 1980) showed longitudinal variations of Young's modulus in four different species of birds (chicken, turkey, pheasant and gull). Bonser and Purslow (Bonser and Purslow, 1995) contributed similar data for a mute swan. Finally, Cameron et al. (Cameron et al., 2003) investigated the axial alignment of keratin molecules along the rachis length. They showed a higher axial alignment and a higher Young's modulus towards the feather's tip in volant (capable of flight) bird species (geese and swans). Interestingly, such variations were absent in the non-volant ostrich. The wide range of reported Young's moduli may be due to the different keratin molecule orientations within the rachis, resulting in an anisotropic material that reacts differently to tension and bending.

Bonser and Purslow (Bonser and Purslow, 1995) were the first to comprehensively study different bird species with the goal of determining the flexural stiffness and the Young's modulus of

feather rachises. These authors performed tensile tests on small parts of feather rachises from eight different species of birds, including the tawny owl (*Strix aluco*, 2.76 GPa) and the pigeon (*Columba livia*, 2.42 GPa). The Young's modulus varied around 2.5 GPa for all species investigated, except for the grey heron (*Ardea cinerea*, 1.78 GPa). No significant differences were found when comparing primaries (p7–p10) within species. However, longitudinal variations of Young's modulus along the length of the rachis were found.

Young's modulus was measured along the rachis length in a primary feather of a mute swan (*Cygnus olor*) (Bonser and Purslow, 1995), and was found to increase towards the tip of the feather. In dynamic bending tests, these variations were influenced by frequency and temperature (*E* was directly proportional to frequency and inversely proportional to temperature). However, the position-, frequency- and temperature-dependent variations were relatively small. Apart from the elastic modulus, Bonser and Purslow (Bonser and Purslow, 1995) investigated the flexural stiffness of feathers. They found that the results of the measurements varied significantly along the length of a primary feather, between primaries of different positions and between species investigated.

Likewise, the geometry of feather shafts has not yet been studied in detail. Available publications report values of the second moment of area in studies about either molting strategies (Weber et al., 2010) or the determination of the bending behavior (Purslow and Vincent, 1978). To our knowledge, a quantitative study that relates material properties and geometrical properties of feathers with flexural stiffness is not available. This study provides quantitative data concerning rachis geometries from barn owls and pigeons.

In general, the shaft of a feather can be expressed as a cantilever beam. The geometry and the profile of such a beam influence the bending behavior. Hollow beams are known to be simultaneously flexible and robust against loading (Klein, 2009). However, these structures tend to buckle under critical loading. Filling the beam with foam, as it is seen in feather shafts, prevents buckling to a certain degree. Variations in the profiles and the appearance of ridges and a transversal septum are further options to influence the bending behavior (Klein, 2009; Purslow and Vincent, 1978). In flight feathers, various adaptations have evolved depending on the requirements concerning force resistance and lift. Purslow and Vincent (Purslow and Vincent, 1978) tested the role of the variation in the second moment of area along the rachis length of pigeon primaries by determining the bending behavior. They claimed that the flexural stiffness is largely controlled by the geometry of cortical regions and their specializations such as cortical ridges and braces.

In this study, data are provided for the Young's modulus of rachis keratin in two species of birds, barn owls [*Tyto alba pratincola* (Bonaparte 1838)] and pigeons (*Columba livia* Gmelin 1789). Furthermore, the distribution of the second moment of area and the calculated flexural stiffness for fifth primaries of both species are presented. We have chosen these species because they are of similar body mass (barn owl, mean ± s.d.=465±15 g; pigeon, 550±97 g; *N*=4), but differ in wing planform, wing and feather size and in some specializations of the feathers (Bachmann et al., 2007).

MATERIALS AND METHODS
Feather material and anatomy of feather shafts
Six fifth primaries (three each from a right wing and a left wing) and one fourth primary (right wing) were obtained from dead barn owls formerly bred and raised in the colony of the Institute for Biology II (RWTH Aachen University, Aachen, Germany) and from five dead pigeons provided by a local breeder. All investigated feathers of each species were of similar size and color. The feathers were taken from specimens that had been used in other experiments under a permit from the local authority [Landespräsidium für Natur, Umwelt und Verbraucherschutz Nordrhein Westfalen (LANUV), Recklinghausen, Germany].

Digital photographs of the feathers were analyzed with respect to the lengths of the rachis and the calamus using Photoshop CS (Adobe Photoshop CS, Adobe Systems, San Jose, CA, USA). The principle cross-sectional profiling of a remex was visualized using one fourth primary of each species, because barn owl feathers are rare and all available fifth primaries were taken for the material analysis. The rachises were cut in unequal sections, disallowing a percentage depiction of the rachis. The fourth primaries, however, were cut every 10% of rachis length and the surfaces of the designated cuts were photographed with a digital camera (Nikon Coolpix 4500, Nikon, Tokyo, Japan) mounted on a stereo-microscope (Nikon SMZ 10A). This combination gave a resolution of 0.19 to 0.47 pixels μm^{-1} depending on the magnification used. The cortices of the rachises and the transversal septi were marked black (RGB: 0, 0, 0) and the surroundings white (RGB: 255, 255, 255) using Photoshop CS. All photos were exported in TIFF format to avoid compression errors. Shape, size and specializations, such as dorsal ridges and transversal septi, were identified and described for each cross-sectional profile.

Material properties
Material properties were obtained from all fifth primaries. Each rachis of the fifth primaries was divided into discrete parts for further analysis with two individual methods, a two-point bending test and nanoindentation. Feathers from barn owls were cut into nine parts, and feathers from pigeons were cut into seven parts because of the smaller feather length. The segmentation is shown schematically in Fig. 1. Here, rachis samples for nanoindentation were 10 mm long

Fig. 1. Schematic drawing of the sampling of nanoindentation and bending test specimen. (A) Complete feather. (B) Feather rachis after removing the vane with scissors. (C) Specimen for nanoindentation (length: 10 mm each). (D) Specimen for two-point bending tests (length: 40 mm with the exception of the most distal part of pigeon feathers, which was 30 mm).

and rachis samples for bending tests were 40 mm long, except for the most distal parts of the pigeon rachises, which were 30 mm in length. The residual most distal part of the rachis, used for nanoindentation, varied in length (barn owl, 13.13–19.84 mm; pigeon, 8.14–12.38 mm) because of the different lengths of the feathers.

Method I: two-point bending test

The rachis of a feather can be approximated as a cantilever beam. As such, Young's modulus was calculated after performing two-point bending tests and the measurement of the second moment of area (described in the following subsection).

For the bending test, the rachis parts (see Fig. 1D) were prepared using scissors to remove the lateral vanes to 1 mm adjacent to the central shaft, which prevented the shaft from being damaged. Afterwards, each specimen of the rachis was fixed with super glue (UHU sekundendkleber, UHU GmbH and Co. KG, Bühl/Baden, Germany) to an aluminum block. A hole was drilled into the aluminum block, which was as thick as the inserted rachis diameter to avoid adverse effects from the super glue used to fix the feather into place, e.g. the influence of the unknown material properties of the super glue on the overall bending behavior of the rachis samples. The aluminum block was mounted to a micro-manipulator (Märzhäuser MM33, Wetzlar, Germany) to guarantee the exact positioning of the specimen onto a micro-scale (Mettler Toledo XS 205, Mettler Toledo AG, Greifensee, Switzerland) and a precise deflection during the bending tests. On the measuring side, the rachis touched a thin metal membrane (blunt razor blade) that was flexibly fixed on the scale pan. This prevented the rachis from slipping over the metal membrane during the deflection, which would change the test length (Fig. 2).

The test length (*l*) of all specimens was set to be 30 mm except for the most distal specimens of the pigeon feathers, in which case the test length was 25 mm due to the rachis length. Each specimen was manually driven towards the scale until the lower surface of the rachis touched the metal membrane slightly. The specimen was then deflected by 1 mm and the rising force (*F*) was measured. The force value was measured immediately after the deflection distance

[*w*(*x*)] was reached, because hysteresis effects of the material were observed in preliminary experiments and the force values changed quickly after deflection. Owing to the hysteresis, the individual material-characterizing measurements for each specimen were measured after at least 12 h, during which the material had completely recovered. The bending tests were repeated eight times for each rachis part. It is known that the elastic properties of β-keratins, of which feathers are mainly composed, appear somewhat conservative when tested at room temperature and humidity (Taylor et al., 2004). Hence, the specimens were stored and all experiments were performed in a laboratory under almost constant climatic conditions (22.2±0.4°C, 28.2±0.9% humidity) to avoid an influence of temperature and humidity on the results.

Hysteresis effect

Many biological materials show a viscoelastic behavior after mechanical treatment (Fraser and Macrae, 1980; Bonser and Purslow, 1995). We found a hysteresis effect of the keratin in preliminary two-point bending experiments as well. This effect was investigated in one experiment of extended duration. One rachis of the barn owl was deflected for a given time. The decreasing force was measured at regular 10 s intervals for the first 30 min, followed by 600 s intervals for 2 h. In an additional test, 6 h passed until the material was completely restored after the bending force was removed. To avoid artifacts caused by the hysteresis, each individual specimen used in the two-point bending test was examined after a time interval of at least 12 h to let the material fully recover.

Determination of the second moment of area

Subsequent to the bending tests, the test length of each rachis part was cut into three similarly sized pieces. Hence, four cross-sections of each rachis part were obtained, for which the second moment of area (*I*) was calculated as follows.

Digital photographs of the cross-sections were taken with a high-resolution digital camera (Nikon Coolpix 4500, Nikon Corp., Tokyo, Japan) mounted on a stereo-microscope (Nikon SMZ 10A). Further analysis was performed using Photoshop and MATLAB (The MathWorks, Natick, MA, USA). First, the cortex of the rachis and the transversal septum was marked black (RGB: 0, 0, 0) and the surroundings white (RGB: 255, 255, 255) for all photographs taken. The air-filled cells (substantia medullaris) within the cortex were not taken into account because their influence on force production are most likely negligible. In comparison to the cortex of the rachis, the area formed by the cell walls is relatively small. The cells are distributed close to the neutral axis of bending, and Young's modulus of the substantia medullaris is quite small (Bonser, 2001). The effect of the substantia medullaris on the total flexural stiffness is likely negligible for the small deflection distance (1 mm) during bending.

The second moment of area was measured according to a method provided by Baron et al. (Baron et al., 1997). Their approximation of the second moment of area uses finite pixel information from pictures of beam cross-sections for the calculations. The second moment of area *I* at a given position along the rachis is given by:

$$I = \sum_{i=0}^{\text{all 'black' pixels}} y_i^2 \, dA \,, \tag{1}$$

where y_i represents the distance of the *i*th pixel from the neutral axis and d*A* is the area of one pixel.

For the implementation of this formula in MATLAB, the neutral axis, the line that passes through the centroid of mass of the cross-
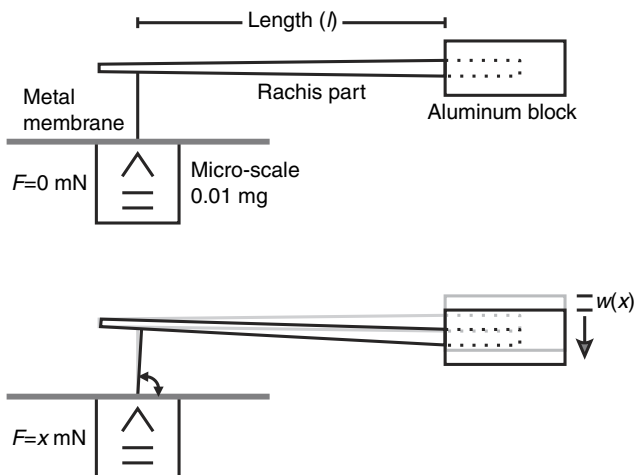

Fig. 2. Schematic of the two-point bending test. (A) The test specimen (rachis) is fixed to an aluminum block that in turn is mounted to a micro-manipulator (not shown). The rachis is positioned at a defined length (*l*) above a micro-scale. (B) Rising forces (*F*) are measured with the micro-scale after displacing the rachis a defined distance, *w*(*x*). At the contact point of the rachis, a metal membrane is flexibly fixed onto the scale pan.

section, had to be found. The centroid was found by taking the average of the positions of all black pixels, as the pixels are of uniform size and density. Because the rachis was bent dorso-ventrally and no torsion was observed, the neutral axis was horizontal.

Next, we obtained the continuous change of I with respect to x by fitting a third-order polynomial $I(x)=ax^3+bx^2+cx+d$ through the four supporting points for each bending specimen.

Calculation of Young's modulus (two-point bending test)

Young's modulus was calculated by applying the formula for the curvature of a beam $w''(x)$, which can be solved with values of Young's modulus, the second moment of area and the bending moment $[M_b(x)]$:

$$M_b(x) = F(x - l). \qquad (2)$$

The equation for the curvature of a beam is taken from Grote and Feldhusen (Grote and Feldhusen, 2007) and is given by:

$$w''(x) = \frac{-M_b(x)}{E\,I}. \qquad (3)$$

Because $w(x)$ was known [deflection of the rachis, $w(x_{max})=1$ mm], the right part of the equation needed to be integrated twice:

$$w(x_{max}) = -\frac{F}{E} \iint \frac{(x-l)}{ax^3+bx^2+cx+d}\,dx^2. \qquad (4)$$

Afterwards, this equation had to be solved for E:

$$E = -\frac{F \iint \frac{(x-l)}{ax^3+bx^2+cx+d}\,dx^2}{w(x_{max})}. \qquad (5)$$

This complex double integral in Eqn 4 was difficult to calculate because of the x in the numerator. To avoid such problems, the term $(x-l)/(ax^3+bx^2+cx+d)$ was plotted and substituted by a sixth-order polynomial $[g(x)=a_nx^n+...+a_1x+a_0]$ using MS Excel (Microsoft Corporation, Redmond, WA, USA). This polynomial was then integrated twice. The argument a_0 of the first and second integration equals zero ($a_0=0$), as $w'(0)$ and $w(0)$ equal zero as well. By insertion of the measured parameters for $w(30)$, $M_b(30)$ and I, the Young's modulus was determined for each rachis part.

Calculation of bending stiffness

The bending stiffness EI is a measure of the relationship between the applied bending moment and the resulting deflection of the beam. It is calculated as the product of Young's modulus (E) and the second moment of area (I). The bending stiffness was calculated for each feather using information about E from the two-point bending tests and information about I from the measurement of the distribution of the second moment of area.

Method II: nanoindentation

Nanoindentation is a method that is well suited to characterize the stiffness of micro- and nano-structured materials. This method was employed to determine the local Young's modulus of small dorsal rachis parts in order to critically evaluate the findings of the two-point bending tests with a second, independent method.

The sampling areas for the test specimens are shown in Fig. 1. In barn owls, five rachis parts per feather were evaluated, whereas four rachis parts for each pigeon feather were analyzed. Thin longitudinal stripes were cut from the dorsal cortex, sharpened at the distal end and embedded in polyester resin (XOR-Giessharz, Hobby-Time Bastel-System GmbH, Neukirch, Germany) that polymerized under room temperature and normal light conditions.

This resin was chosen because it did not require a change in temperature or wavelength, which might have influenced the sample properties in the process of polymerization. After polymerization, the embedded specimens were cut transversely with an ultra-microtome (Reichert OmU3 ultra-microtome, C. Reichert AG, Vienna, Austria) and a glass knife (tip angle=45 deg). Only cuts with an average surface roughness (R_a) <60 nm were taken for the nanoindentation measurements.

Load-displacement data were acquired using a depth-sensing nanoindenter (TriboIndenter, Hysitron Inc., Minneapolis, MN, USA). A Berkovich indenter tip was used for the measurements. The tip of this indenter resembled a pyramid with three faces that had a tip angle of 142 deg and a tip diameter of ~150 nm.

The system was calibrated using a fused silica standard prior to the experiments (Fig. 3). In the measurements, the applied force (F) and displacement (h) of the indenter were recorded simultaneously and subsequently evaluated according to the method of Oliver and Pharr (Oliver and Pharr, 1992). In this method, the slope (dF/dh) of the initial unloading part of the load-displacement curve (Fig. 3) was used to extract the reduced modulus E_r as given by the following equation:

$$\frac{dF}{dh} = \frac{2}{\sqrt{\pi}} E_r \sqrt{A(h_c)}, \qquad (6)$$

where $A(h_c)$ is the contact area under the peak load.

In a further step, the following formula was used to calculate Young's modulus (E):

$$\frac{1}{E_r} = \frac{(1-v_i^2)}{E_i} + \frac{(1-v)}{E}, \qquad (7)$$

where E_i and v_i are the Young's modulus and Poisson's ratio, respectively, of the indenter, and v is the Poisson's ratio of the keratin. Because Poisson's ratio has not been determined for feather keratin so far, it was estimated to be 0.4, the Poisson's ratio of oryx horn (Kitchener and Vincent, 1987). Each specimen was measured 16 times at different positions (array of 4×4 indents) with a maximum load of 9500 μN and a loading rate of 1900 μN s^{-1}. Because Busson et al. (Busson et al., 1999) postulated four structurally distinct layers within the rachis cortex of a peacock feather shaft, indentation experiments in the present study were concentrated on the central parts of the rachis' cortex. Unfortunately,
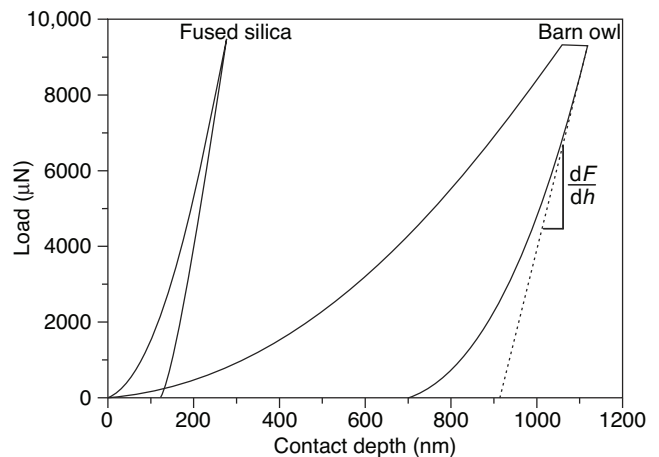

Fig. 3. Example load-displacement curves of nanoindentation tests with barn owl feather keratin and fused silica. Fused silica was used for calibration purposes. dF/dh, slope of the initial unloading part of the load-displacement curve.
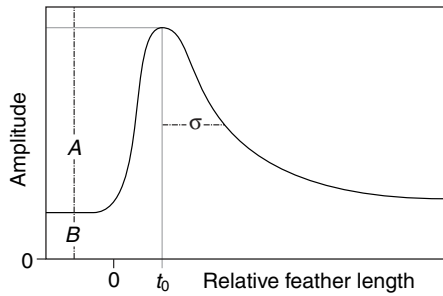
Fig. 4. Example gamma distribution given by amplitude *A*, offset *B*, width δ and relative feather length t_0.

Busson et al. (Busson et al., 1999) did not provide any scaling factor for different positions within the rachis nor for different feathers and species of birds. Thus, it cannot be ruled out that some measurements may have included a structurally different region adjacent to the central part of the rachis cortex. The influence of structural differences on Young's modulus should, however, be small as long as the density is constant (Kurapov et al., 2007; Music and Schneider, 2008).

Statistics

Student's *t*-statistics were calculated for all values that were directly comparable: feather length, calami length, calami percentage length and mean Young's modulus of the two species. A different approach for the statistical analysis had to be found for the second moment of area and local Young's modulus data, as these data were taken at different *x*-values for the two species.

The variation of the second moment of area was fitted by a gamma distribution (Fig. 4):

$$\gamma(t) = \frac{A}{t_{max}^{\gamma-1}e^{(1-\gamma)}}(t - t_0 + t_{max})^{\gamma-1}e^{\frac{-(t-t_0+t_{max})}{\sigma}} + B . \quad (8)$$

The gamma function was defined by the following parameters: amplitude *A*, offset *B*, width σ and relative feather length t_0 (equivalent to the maximum of the data), for $t>t_0-t_{max}$ and $\gamma(t)=0$, where $t_{max}=\sigma(\gamma-1)$. Note that the coefficient γ is a shape parameter and was not fitted but remained fixed at a value of 3.

It was not possible to fit the curves of Young's modulus owing to the few data points available. Instead, a Kruskal–Wallis test was performed to determine whether there were any statistical differences between the two methods used or between the two species investigated. In the case of significance, closely related data points were compared using Dunn–Sidak *post hoc* tests.

Data are presented as means ± s.d. unless otherwise specified.

RESULTS
Anatomy of the rachis of barn owl and pigeon primaries

The length of the rachises differed significantly between the two species. The fifth primaries of pigeons were shorter in length than the fifth primaries of barn owls (pigeon, 152.5±4.3 mm; barn owl, 219.5±3.1 mm; *t*-test: *P*<0.0001, d.f.=10, *N*=6). Interestingly, the calami of the fifth primaries were not statistically different in length (pigeon, 35.5±1.2 mm; barn owl, 34.7±1.4 mm; *t*-test: *P*=0.292, d.f.=10, *N*=6; Fig. 5). However, the comparison of the percentage length of the calamus in relation to the rachis showed a statistically significant difference between the two species (pigeon, 23.29±1.13%; barn owl, 15.8±0.69%; *t*-test: *P*<0.0001, d.f.=10, *N*=6).

The feather shafts of the fifth primaries of the two species had some geometrical features in common, but differed in some anatomical aspects as well. Two fourth primaries of the two species were analyzed to show profile changes within the rachis in principle (Fig. 5). These feathers have an anatomy comparable to that of fifth primaries.

The calami of primary feathers were attached to the bird's skin. Cross-sections of the pigeons' calami had a round to elliptic shape (Fig. 5B, first and second profile from below), whereas cross-sections
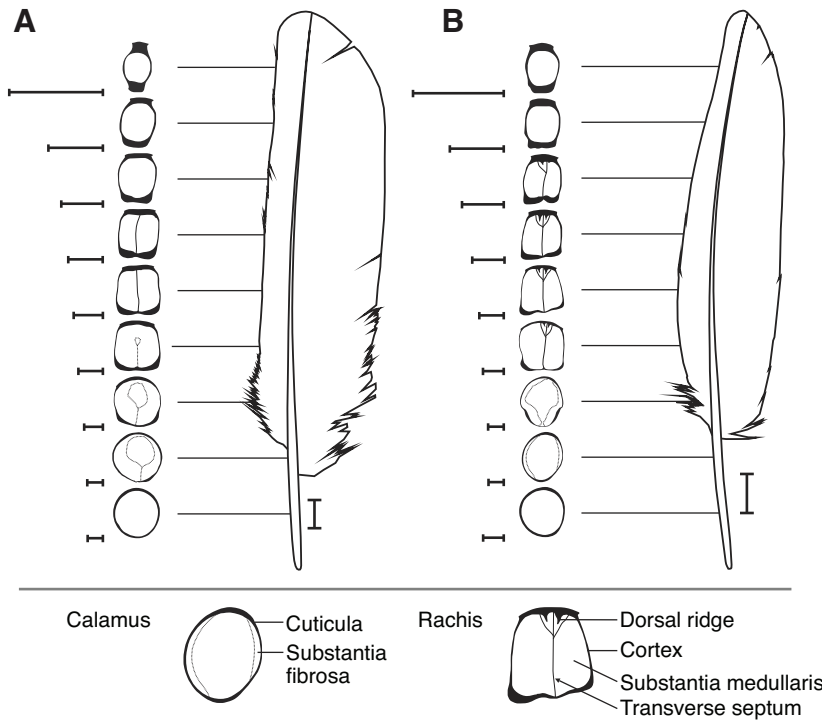

Fig. 5. General cross-sectional shape of the shaft of a fourth primary of the barn owl (A) and the pigeon (B). The feathers are normalized by their length for better comparison. Elements of the shaft are named at exemplary cross-sections (bottom). Scale bars represent 1 mm each for all cross-sections and 10 mm for the feather drawings.

of barn owls' calami were almost round (Fig. 5A, first profile from below). In both species, the inner sidewalls of the calamus next to the vanes were covered by a foam-like structure termed the substantia fibrosa. The proximal end of the calamus was attached to the carpometacarpus bone. The postpatagium with its strong tendons connected calami of neighboring feathers.

The cortex (outer region) of the rachis had a more or less rectangular shape in the two species. The hollow cortex was filled with a foam-like structure as well, termed substantia medullaris, which was similar to the substantia fibrosa. Dorsal and ventral parts of the cortex were thicker compared with the sidewalls where the vanes emerged (Fig. 5). The cross-sectional shape of the rachis cortex differed between the two species in some detail. In barn owls, the cortex was smooth on the inner as well as on the outer contour (Fig. 5A). The only exception was a small spine or ridge observed at the inner ventral side between 30 and 50% of the rachis length. A membranous structure, termed the transversal septum, emerged from this spine. The transversal septum was oriented dorso-ventrally and ended within the medulla or at the smooth inner dorsal cortex (Fig. 5), depending on the position examined.

A similar spine was found at the ventral cortex of the pigeon's feather, and it also supported a transversal septum. However, the transversal septum of pigeons' remiges had a richer structural appearance with several branches. In pigeons, the branches of the transversal septum terminated at the inner dorsal sidewall, where they merged with dorsal spines. These dorsal spines first formed four, and later two, longitudinal ridges on the inner dorsal cortex between 40 and 70% of the feather's length (Fig. 5, upper right). Although the ridges had a strong appearance at proximal parts of the feather, they faded out towards the feather's tip. Such ridges were totally absent in all barn owl feathers investigated.

Second moment of area

The analysis of profiles provided quantitative data for I along the rachis length. In Fig. 6, the values of I are plotted against the percentage length of the rachis. I equaled zero at 0 and 100% of the length of the rachis in both species (data not shown).

The mean values of I estimated by the gamma fit were always higher in barn owl feathers than in pigeon feathers (Fig. 6). These differences were statistically significant between 0 and 79% of the length of the rachis (see Table 1), when estimated data from the gamma fits were compared. At first glance, the gamma function described the data very well (all $R^2 \geq 0.98$; Fig. 7). Although the

Table 1. Student's t-test results of the comparison of calculated second moment of area (I) from gamma fits of barn owl and pigeon data along the feather shaft

Length of feather shaft	I		P
	Pigeon	Barn owl	
5.3	0.835	2.128	<0.0001
6.6	1.060	2.204	<0.0001
9.7	1.503	2.292	<0.0001
13.1	1.734	2.254	0.0010
14.3	1.764	2.215	0.0034
18.8	1.686	1.994	0.0397
19.7	1.649	1.944	0.0474
26.1	1.252	1.520	0.0482
28.4	1.105	1.375	0.0359
32.8	0.832	1.103	0.0164
37.4	0.599	0.859	0.0066
39.5	0.512	0.764	0.0045
41.8	0.425	0.663	0.0029
45.9	0.306	0.517	0.0015
51.2	0.196	0.367	0.0007
52.5	0.176	0.337	0.0006
55.8	0.133	0.270	0.0005
59.0	0.102	0.218	0.0004
60.4	0.091	0.197	0.0004
62.6	0.076	0.169	0.0005
72.3	0.036	0.083	0.0029
74.2	0.032	0.072	0.0058
77.0	0.027	0.058	0.0175
78.8	0.025	0.051	0.0360
81.5	0.022	0.041	0.0981
83.3	0.020	0.036	0.1745
86.2	0.018	0.028	0.3635
87.9	0.017	0.025	0.4977

Second moment of area data are means (N=6, d.f.=10).

coefficient of determination provides a measure for the quality of a fit in linear models, it was used as an indicator of whether the resulting fit parameters of the individual fits were comparable to each other.

The gamma functions were used to calculate data at missing x-values for the relevant species (Fig. 7). Significant differences between barn owl and pigeon specimens were found using Student's t-test (all $P \leq 0.05$, N=6, feather length between 5 and 79%; not significant above 79%; Table 1).

The comparison of the fit parameter of the gamma distributions revealed statistically significant differences concerning three shape parameters: t_0, amplitude and width (Table 2). Offset, e.g. the shift parallel to the x-axis, showed no statistically significant differences (MANOVA, fixed factor=bird species (barn owl or pigeon), independent variables=t_0, amplitude, width, offset; P=0.0006; for details see Table 2).

Although values of I differed between the two species, the change in I along the feathers' length was alike in both species in that it was dependent on the percentage length of the feathers. I increased towards 2.49 ± 0.13 mm^4 within the first 10% of feather length in barn owls and towards 1.74 ± 0.37 mm^4 within the first 20% of feather length in pigeons (Fig. 6). From here, I decreased exponentially towards the tip of the feather in both species.

As mentioned before, the highest values of I were found at the calamus, more specifically at 75.0% of the calamus length in pigeons and at 61.6% of the calamus length in barn owls (Fig. 5). Here, strong tendons of the postpatagium connected calami of neighboring feathers of the relevant species of birds.
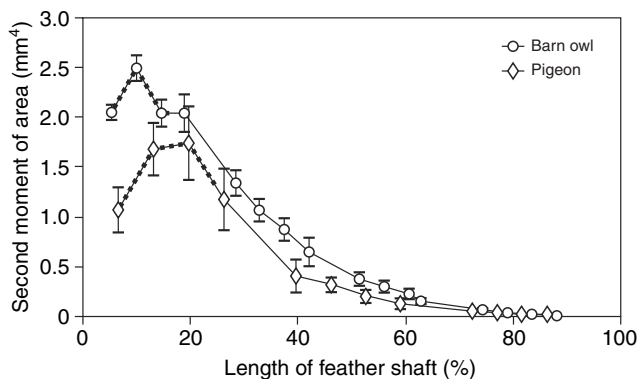

Fig. 6. Longitudinal variation of the second moment of area of feather shafts from barn owl and pigeon fifth primaries. The lengths of the calami are indicated by the bold dotted lines at the most proximal part of the rachis. Data are means ± s.d. (N=6 for each species).
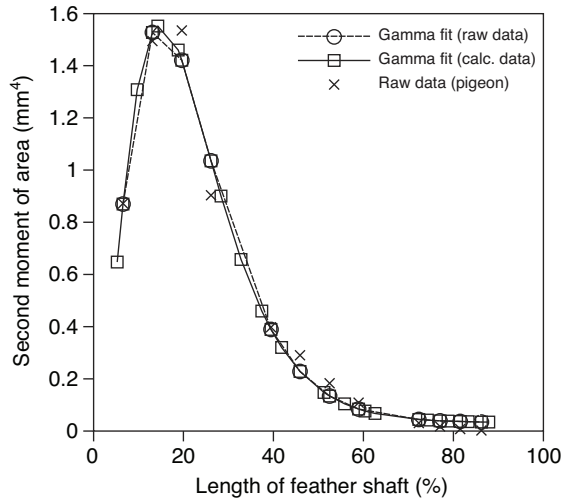
Fig. 7. Example fitting result for the gamma function, using raw data from pigeons (crosses), gamma fit of raw data from pigeons and barn owls (open circles, dashed line) and gamma fit of calculated mean data of feather positions from pigeons and barn owls (open squares, solid line).
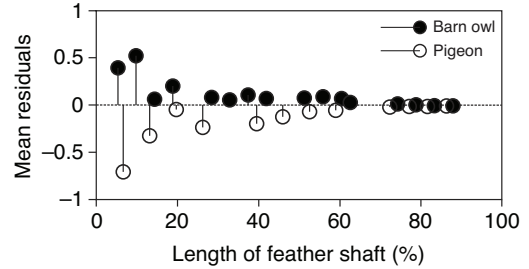

Fig. 8. Mean of residuals (second moment of area) for barn owl (filled circles) and pigeon (open circles) data along the percentage length of the feather shaft.

at the base of the feather, the highest values (barn owl, 6.33±1.29 GPa; pigeon, 6.38±0.75 GPa) were obtained at the tip of the feather (Fig. 9). The increase in Young's modulus of approximately 50% was statistically significant in both species (t-test: barn owl, P=0.0033, d.f.=10, N=6; pigeon, P=0.0003, d.f.=10, N=6).

Nanoindentation

The local Young's modulus of keratin was measured by nanoindentation. Rachis parts that lay between the bending test samples were investigated. Fig. 6 shows Young's modulus values as a function of the length of the feather shaft. The mean Young's modulus of barn owl feather keratin was 6.54±0.82 GPa, whereas the mean value for keratin from the pigeon was 5.96±1.52 GPa. Statistically, the pooled mean values were not significantly different (t-test: P=0.1524, d.f.=33) between the two species.

The Young's modulus data were further statistically analyzed with respect to differences between the species investigated and between the methods used. First, the differences between the Young's moduli measured with nanoindentation (method I) and bending tests (method II) were investigated for each species by means of a Kruskal–Wallis test (Table 3). Next, the same method was used to compare results from nanoindentation of barn owl feathers with pigeon feathers. Finally, the Young's modulus results from the bending test of barn owl and pigeon feathers were compared. As

In a second approach, the pooled data for each species were fitted to the gamma function mentioned above and the means of the residuals were calculated (Fig. 8). Applied Student's t-tests yielded statistical differences between barn owl and pigeon for the whole length of the feather shaft (P=4.8207e–004, d.f.=26), and parts of the feather shaft: 0–25% (P=0.0221, d.f.=5), 25–50% (P=3.1952e–004, d.f.=5), 50–75% (P=0.0033, d.f.=6), 75–100% (P=0.0279, d.f.=4).

Determination of Young's modulus
Two-point bending test

The pooled mean values of the measured Young's modulus did not vary significantly between two species (barn owl, E=5.45±1.21; pigeon, E=5.39±1.07; t-test: P=0.87, d.f.=37, N_{owl}=22, N_{pigeon}=17). However, longitudinal variations occurred. Although the smallest values (barn owl, 4.2±0.4 GPa; pigeon, 4.4±0.4 GPa) were found

Table 2. Results of MANOVA with total, between and within sum of squares for four fit parameters [relative feather length (t_0), amplitude, width and offset] comparing barn owl and pigeon data

| | | Sum of squares | | | | | | |
	t_0	Amplitude	Width	Offset	d.f.	Mean square	F	P
Between								
t_0	**70.73**	−7.87	−35.84	0.2	1	70.728	35.982	0.0001
Amplitude	−7.87	**0.88**	3.99	−0.02	1	0.876	20.125	0.0012
Width	−35.84	3.99	**18.16**	−0.1	1	18.157	44.583	0.0001
Offset	0.2	−0.02	−0.1	**0**	1	0.001	1.167	0.3054
Within								
t_0	**19.66**	1.19	−1.95	−0.04	10	1.966		
Amplitude	1.19	**0.44**	0.42	−0.02	10	0.044		
Width	−1.95	0.42	**4.07**	−0.08	10	0.407		
Offset	−0.04	−0.02	−0.08	**0.01**	10	0.001		
Total								
t_0	**90.39**	−6.68	−37.78	0.17	11			
Amplitude	−6.68	**1.31**	4.41	−0.04	11			
Width	−37.78	4.41	**22.23**	−0.18	11			
Offset	0.17	−0.04	−0.18	**0.01**	11			

Also shown are the mean square, F-value and probability derived from the cumulative density function of F for the diagonal values (bold).
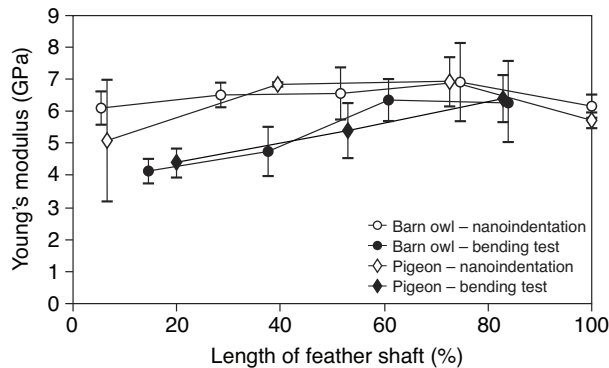
Fig. 9. Longitudinal variation of the Young's modulus of feather rachis keratin of fifth primaries from barn owls and pigeons. Results obtained with two independent methods are shown: nanoindentation (open symbols) and the two-point bending test (filled symbols) (N=6).
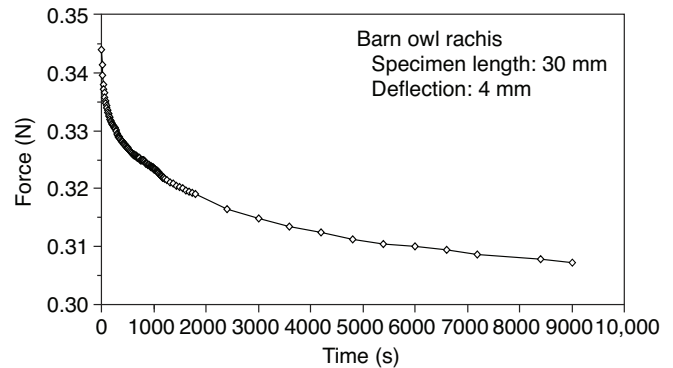

Fig. 10. Hysteresis effect of feather keratin. The time-dependent force decrease was measured at one fourth primary of the barn owl with a given deflection of 4 mm (N=1).

the differences were statistically significant for all four testing conditions, which means that there are differences within the data set, a *post hoc* Dunn–Sidak test was applied. This showed that closely related data points were not significantly different in all four cases, except for the comparison of the two methods at barn owl data. Here, differences were found between 14.4 and 51.2% of the length of feather (Dunn–Sidak test: $P{\leq}0.05$).

More interestingly, significant differences were found between the proximal and distal feather parts of within a species or method. Young's modulus of proximal feather regions was significantly lower than of distal regions in both species.

Measurement of hysteresis effect
The hysteresis curve after extensive deflection is depicted in Fig. 10. Although the measured force decreased continuously and quickly in the first hour, the curve flattened as time passed. After 2.5 h (9000 s), no further changes were observed.

Bending stiffness
The empirical Young's modulus from the bending tests was used to calculate longitudinal changes in the bending stiffness (Fig. 11). Because I had a higher variation along the feather length than E, its influence on the bending stiffness was higher as well. According to the second moment of area, the highest values (barn owl, $10.31{\pm}0.79\,\mathrm{N\,mm^2}$; pigeon, $7.62{\pm}1.55\,\mathrm{N\,mm^2}$) were found within the calami of the two species. From here, the bending stiffness decreased towards the tip of the feather, but somewhat slower than the second

moment of area because of the increase in E towards the tip of the feather (Fig. 11).

DISCUSSION
Primary feathers in barn owls and pigeons were investigated with respect to their rachis geometry and changes in the Young's modulus of keratin along the rachis length. The Young's modulus of feather keratin from fifth primaries was determined using both two-point bending and nanoindentation tests in both species. Statistically significant interspecific differences of Young's modulus of feather keratin were not found. The Young's modulus values measured with the two methods did not differ significantly, except for those values calculated between 14.4 and 51.2% of the length of the feather in the barn owl (Dunn–Sidak test: $P{\leq}0.05$). However, differences in Young's modulus between proximal and distal feather regions were found in both species.

Values of the second moment of area and the resulting bending stiffness were always higher in barn owls than in pigeons relative to the normalized lengths of the feathers. This finding was statistically significant between 0 and 79% of the length of feather. In this context, the geometry of the feather shafts differed distinctively between the two species.

In the following sections, the two methods that were employed will be discussed, and the Young's modulus of rachis keratin data will be discussed with reference to values found in the literature. Finally, the relative importance of geometry *versus* bending stiffness of the feather shafts will be discussed.

Table 3. Results from Kruskal–Wallis tests on the differences between the Young's moduli measured with nanoindentation and bending tests for barn owls and pigeons

| Species/method	Comparison	Source	Sum of squares	d.f.	Mean square	χ^2	P
Pigeon	Methods	Groups	88,622.588	6	14,770.431	43.981	7.46e–08
		Error	221,687.412	148	1497.888		
		Total	310,310	154			
Barn owl	Methods	Groups	1,071,468.95	8	133,933.619	86.072	2.91e–15
		Error	3,721,202.05	377	9870.562		
		Total	4,792,671	385			
Nanoindentation	Species	Groups	2,233,584.829	8	279,198.104	106.998	1.57e–19
		Error	8,183,040.171	491	16,666.070		
		Total	10,416,625	499			
Two-point bending test	Species	Groups	2982.117	6	497.019	20.787	0.002
		Error	2756.383	34	81.070		
		Total	5738.5	40			
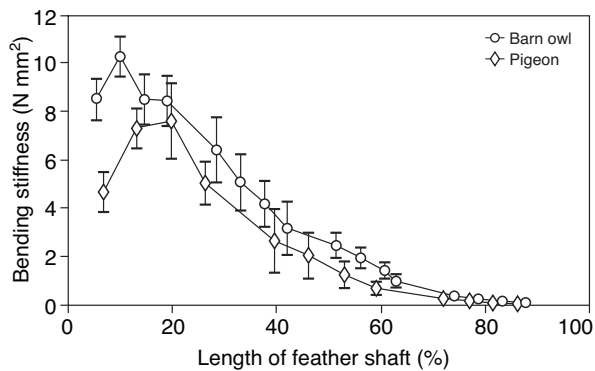
Fig. 11. Longitudinal variation of the bending stiffness of rachises of fifth primaries from barn owls and pigeons (*N*=6).

Comparison of methods employed

In this study, two independent methods were used to determine the Young's modulus of feather keratin from barn owls and pigeons. Each method requires different specimen sizes. In bending tests, 30 mm long feather segments were used to estimate Young's modulus, whereas the volume deformed during nanoindentation is of the order of $10\,\mu m^3$. Hence, global values of Young's modulus were determined by bending tests, whereas the local elastic properties were determined during nanoindentation.

The orientation of the keratin molecules might play an important role in bending tests. Cameron et al. (Cameron et al., 2003) investigated geese, swan and ostrich feathers with respect to Young's modulus and the orientation of the keratin molecules along the rachis length. In volant birds, Young's modulus increased with a higher axial alignment of the keratin molecules towards the feather's tip. Such trends were absent in ostrich feathers as there was no alignment of the molecules towards the feather's tip. Changes in the axial alignment of the keratin molecules might be responsible for the different values of Young's modulus measured with the bending test. Here, tensile and compression stresses differed with the varying orientation of the molecules. In nanoindentation measurements, the density of the material is much more important than the orientation of the molecules. In cases where the density distribution of keratin molecules along the rachis is homogeneous, the orientation of the keratin molecules should have a much higher impact on the data of the bending tests compared with data determined from nanoindentation.

Apart from this difference, some assumptions had to be made in order to calculate Young's modulus from the bending test results, which may have influenced the results. The two-point bending test is an established method to determine mechanical and material properties. Normally, a solid beam with a constant cross-section is formed from the material and further analyzed with machine-aided setups. This procedure was not possible with feather shafts. To determine the Young's modulus of feather keratin, the structure had to be analyzed as a whole. Consequently, heterogeneities of the second moment of area within the specimen were measured and approximated by a third-order polynomial (see Materials and methods). Although the fitting worked well, small errors remained. In this context, the cortex that is filled with a foam-like structure, the substantia medullaris, poses a challenge. Purslow and Vincent (Purslow and Vincent, 1978) removed the medullary foam manually. The loss of the substantia medullaris resulted in a loss of dorso-ventral stiffness of 16.1% and a loss of lateral stiffness of 7.8%. It remained unclear to what extent the removal of the foam-like structure changed the cortices. Specifically, the dorsal ridges and the well-pronounced transversal septum of pigeon feathers might have been damaged in the study by Purslow and Vincent (Purslow and Vincent, 1978). Furthermore, it is unknown whether removing the medulla changed the humidity of the keratin and, hence, influenced the values of Young's modulus, as wetting does have an influence on the material properties of keratin, as shown previously (Kitchener and Vincent, 1987; Taylor et al., 2004).

It is assumed that the substantia medullaris has only a small impact on the measurements, particularly when working with such a small displacement (1 mm) as in the present study. In relation to the cortex, the cell walls of the medullary cells are very thin. Therefore, the small cross-sectional area does not contribute much to the overall second moment of area. Additionally, Young's modulus of the substantia medullaris seems to be relatively weak in comparison to that of the cortex (Bonser, 2001). Hence, the substantia medullaris was left in place for the present study, but was not included in the calculations of the second moment of area.

Nanoindentation is a method well suited to the investigation of elastic and plastic material properties of micro-structured materials (Oliver and Pharr, 1992). Surface roughness critically determines the quality of the nanoindentation data. Therefore, a sample preparation methodology was developed that insured surface average roughness values <60 nm. This effectively reduced the scatter of the measurement data. Furthermore, as nanoindentation provided values of the reduced Young's modulus E_r, Poisson's ratio is required to calculate Young's modulus E. However, to our knowledge, no values for Poisson's ratio of feather keratin are published. Published values of several structurally related materials range from 0.35 to 0.4 [0.4 for oryx horn (Kitchener and Vincent, 1987), 0.38 for bovine claw horn (Franck et al., 2006) and 0.35 for dry wool fibers (Fraser and Macrae, 1980)]. Although feather keratin differs from other keratin (Stettenheim, 2000), a Poisson's ratio of 0.4 [oryx horn (Kitchener and Vincent, 1987)] was utilized to calculate Young's modulus. A decrease in Poisson's ratio to 0.35 [dry wool fibers (Fraser and Macrae, 1980)] would increase Young's modulus by 4%.

Material properties of feather keratin

The mean Young's modulus of feather keratin for barn owl and pigeon fifth primaries ranged between 4.14 and 6.93 GPa depending on the position measured and the method used. The estimation of Young's modulus of feather keratin from pigeons by Purslow and Vincent (Purslow and Vincent, 1978) yielded slightly higher values [E=7.75–10 GPa (Purslow and Vincent, 1978)]. These authors used bending tests as well, in contrast to Bonser and Purslow (Bonser and Purslow, 1995), who used tensile tests and measured values of E of approximately 2.5 GPa. However, the values of Young's modulus in the present study did not vary statistically significantly between species, which is consistent with the findings of Bonser and Purslow (Bonser and Purslow, 1995). These authors proposed that the small variation in Young's modulus in all species investigated resulted in a large variety of cross-sectional profiling of feather rachises that are perfectly adapted to the individual requirements of the flight apparatus of the particular species. The results of the geometrical variation of barn owl and pigeon rachises support this hypothesis.

Macleod (Macleod, 1980) observed longitudinal variations along the rachis of contour feathers of four bird species (brown chicken, turkey, pheasant and herring gull) in tensile and bending tests. The stiffness increased towards the tip of the feather. A similar observation was made along the rachis of a mute swan's (*Cygnus*

olor) primary feather by Bonser and Purslow (Bonser and Purslow, 1995). These data are consistent with our observations. Functionally, the increase of Young's modulus and the decrease of second moment of area towards the feather's tip ensure a reduced mass and coincidentally guarantee the necessary stiffness. Hence, the bird can beat its wings at higher frequencies and potentially save energy (Rayner, 1993). The reduced thickness results in a reduction of profile drag, which in turn reduces the power requirement during flight (Bonser and Purslow, 1995; Rayner, 1993). Furthermore, the increase in Young's modulus towards the feather's tip might counteract wearing and fatigue effects during resting and, in the case of birds of prey, during striking.

Geometry of feather shafts

Barn owl feathers are generally larger than pigeon feathers (Bachmann et al., 2007). Interestingly, the calami of pigeons were relatively longer than the calami of barn owls. Both species of birds are of a comparable body mass; however, the wings of barn owls are much larger, which results in a very low wing loading of $33.0\,\mathrm{N\,m^{-2}}$ (Bachmann et al., 2011). The low wing loading enables the owl to fly slowly without beating its wings at high frequencies. Pigeons have to beat their wings intensively in order to become airborne. A clap and fling mechanism, which produces additional lift, is also present in these birds (Nachtigall and Rothe, 1982). In conclusion, the intense beating of the wings during flapping flight results in high forces acting on the feather's base, which in turn needs support by muscles and tendons.

The geometry of the rachises differed between the two bird species investigated. The cortex of the barn owl's rachises was not structured internally and the transversal septum was less pronounced, whereas the cortex of the pigeon's rachises comprised small ridges on the inner dorsal side. Additionally, the transversal septum was distinctly developed in pigeon feathers and showed several branches. The calculated bending stiffness was highest within the calamus. Here, large loads are expected because of the long lever arm of the feather. Forces that act on the feather during flight are redirected towards the bones and tendons of the wing. In the range of the highest bending stiffness, strong fibers interconnect the feathers within the postpatagium (Proctor and Lynch, 1993).

The differences in geometry influence the bending behavior under loading and might be an adaptation to the different requirements of the flight apparatus of the two bird species (Purslow and Vincent, 1978). Barn owls fly slowly over vegetation while searching for prey (Mebs and Scherzinger, 2000; Taylor, 1994). The slow flight is enabled by a large wing area that is due to large feathers (Bachmann et al., 2007), which in turn results in low wing loading (Bachmann et al., 2011; Johnson, 1997). Consequently, mechanical loadings in the dorso-ventral as well as in the lateral direction are low. However, high lift is not always an advantage. During hunting, barn owls perform flight maneuvers by acceleration and deceleration with tight turning radii (Brand and Seebaß, 1994; Mebs and Scherzinger, 2000; Neuhaus et al., 1973; Taylor, 1994). In these situations, the lift produced by the wings has to be controlled dynamically. If the forces acting on the feathers exceed a critical value, the angle of attack will change rapidly because of the torsion of the feathers (Rüppell, 1980), thereby changing the profile of the wing and thus the lift. Such behavior can be seen in landing owls. This bending–torsion effect can be actively initiated, whereas the actual torsion is a passive movement of the feather shaft (Carruthers et al., 2007; Rüppell, 1980). The bending–torsion linkage is mainly provided by the geometry, more precisely by the cross-sectional shape of the shaft. As mentioned

previously, dorsal and ventral parts of the rachis' cortex are thickened in relation to the sidewalls, and the transversal septum that spans the dorsal and ventral cortex is only slightly pronounced in barn owls. This leads to a beam structure, which is easy to bend and twist and thus can easily react to changing airflow conditions.

Pigeons are fast and persistent flying birds (Alerstam et al., 2007; Pennycuik, 1968). Their wing area is much smaller than that of barn owls (Johnson, 1997; Pennycuik, 1968), e.g. because of smaller and narrower feathers (Bachmann et al., 2007). As pigeons have the same body mass as barn owls, their wing loading is much higher $(96.8\,\mathrm{N\,m^{-2}})$ (Bachmann et al., 2011). Therefore, pigeons have to beat their wings at high frequencies to become airborne (Berg and Biewener, 2006; Berg and Rayner, 1995; Tobalske and Dial, 1996), which in turn results in high forces acting on the feathers. Consequently, higher dorso-ventral as well as lateral forces are expected in pigeons compared with barn owls. Pigeon feathers are medium-sized and narrow (Bachmann et al., 2007) with a stiff appearance. The dorsal and ventral sidewalls of the shaft are thickened, as was found in barn owls. In contrast to barn owls, the cortex profiles of pigeon feathers were structured. Small ridges run along the dorsal and ventral inner cortex. Additionally, the transversal septum is well pronounced and shows several branches. Such devices stiffen the feathers in the dorso-ventral and rotatory directions, but do not strongly influence lateral movements. Bending stiffness in the lateral direction seems to be controlled by the increased anterior ventral cortex. Such thickening might influence the lateral bending behavior, as this structure is located near the leading edge of the feather and thus has to withstand high aerodynamic forces induced by drag.

This study provides data about the material properties and geometry of the primary feathers of the barn owl and the pigeon. The results unambiguously show that, despite the 50% increase in Young's modulus, the variation in the second moment of area has a greater effect on the flexural stiffness of the rachis.

LIST OF SYMBOLS

A	area, amplitude of gamma fit
$A(h_\mathrm{c})$	contact area under the peak load of the indenter
B	offset of gamma fit
E	Young's modulus
EI	bending stiffness
E_r	reduced Young's modulus
F	force
h	displacement
I	second moment of area
l	length
$M_\mathrm{b}(x)$	bending moment
R_a	average surface roughness
t_0	relative length of feather (gamma fit)
$w(x)$	deflection distance
δ	width of gamma fit
γ	shape parameter of gamma fit

REFERENCES

Alerstam, T., Rosen, M., Bäckman, J., Ericson, P. and Hellgren, O. (2007). Flight speeds among bird species: allometric and phylogenetic effects. *PLOS Biol.* **8**, 1656-1662.

Bachmann, T., Klän, S., Baumgartner, W., Klaas, M., Schröder, W. and Wagner, H. (2007). Morphometric characterisation of wing feathers of the barn owl (*Tyto alba pratincola*) and the pigeon (*Columba livia*). *Front. Zool.* **4**, 23.

Bachmann, T., Mühlenbruch, G. and Wagner, H. (2011). The barn owl wing: an inspiration for the aviation industry? *Proc. SPIE* **7975**, 1-14.

Baron, P., Fisher, R., Sherlock, A., Mill, F. and Tuson, A. (1997). A voxel based approach to evolutionary shape optimization. In *Evolutionary Computing* (ed. D. Corne and J. L. Shapiro), pp. 251-261. Berlin/Heidelberg: Springer.

Berg, A. and Biewener, A. (2006). Kinematics and power requirement of ascending and descending flight in the pigeon (*Columba livia*). *J. Exp. Biol.* **211**, 1120-1130.

Berg, A. and Rayner, J. M. V. (1995). The moment of inertia of bird wings and the inertial power requirement for flapping flight. *J. Exp. Biol.* **198**, 1655-1664.

Bonser, R. H. C. (2001). The mechanical performance of medullary foam from feathers. *J. Mater. Sci. Lett.* **20**, 941-942.

Bonser, R. H. C. and Purslow, P. (1995). The Young's modulus of feather keratin. *J. Exp. Biol.* **198**, 1029-1033.

Boswick, K. and Brady, M. (2002). Phylogenetic analysis of wing feather taxis in birds: macroevolutionary patterns of genetic drift. *Auk* **119**, 943-954.

Brand, T. and Seebaß, C. (1994). *Die Schleiereule.* Wiebelsheim: Aula Verlag.

Busson, B., Engström, P. and Doucet, J. (1999). Existence of various structural zones in keratinous tissues revealed by X-ray microdiffraction. *J. Synchrotron Radiat.* **6**, 1021-1030.

Cameron, G., Wess, T. and Bonser, R. H. C. (2003). Young's modulus varies with differential orientation of keratin in feathers. *J. Struct. Biol.* **143**, 118-123.

Carruthers, A. C., Thomas, A. L. R. and Taylor, G. K. (2007). Automatic aeroelastic devices in the wings of a steppe eagle *Aquila nipalensis. J. Exp. Biol.* **210**, 4136-4149.

Corning, W. R. and Biewener, A. A. (1998). *In vivo* strains in pigeon flight feather shafts: implication for structural design. *J. Exp. Biol.* **201**, 3057-3065.

Crenshaw, D. (1980). Design and materials of feather shafts: very light, rigid structures. *Symp. Soc. Exp. Biol.* **43**, 485-486.

Ennos, A. R., Hickson, J. R. E. and Roberts, A. (1995). Functional morphology of the vanes of the flight feathers of the pigeon (*Columba livia*). *J. Exp. Biol.* **198**, 1219-1228.

Franck, A., Cocquyt, G., Simoens, P. and De Belie, N. (2006). Biomechanical properties of bovine claw horn. *Biosyst. Eng.* **4**, 459-467.

Fraser, R. D. and Macrae, T. P. (1980). Molecular structure and mechanical properties of keratins. *Symp. Soc. Exp. Biol.* **32**, 211-246.

Grote, K.-H. and Feldhusen, J. (2007). *Dubbel – Taschenbuch für den Maschinenbau.* Berlin/Heidelberg/New York: Springer.

Johnson, D. (1997). Wing loading in 15 species of North American owls. In *Biology and Conversation of Owls of the Northern Hemisphere: 2nd International Symposium, Gen. Tech. Rep. NC-190* (ed. J. R. Duncan, D. H. Johnson, T. H. Nicholls), pp. 553-561. St Paul, MN: US Department of Agriculture, Forest Service, North Central Forest Experiment Station.

Kitchener, A. and Vincent, J. F. V. (1987). Composite theory and the effect of water on the stiffness of horn keratin. *J. Mater. Sci.* **22**, 1385-1389.

Klein, B. (2009). *Leichtbau-Konstruktion.* Wiesbaden: Vieweg and Teubner Verlag.

Kurapov, D., Reiss, J., Trinh, D. H., Hultman, L. and Schneider, J. M. (2007). Influence of the normalized ion flux on the constitution of alumina films deposited by plasma-assisted chemical vapor deposition. *J. Vac. Sci. Technol. A* **25**, 831-836.

Macleod, G. (1980). Mechanical properties of contour feathers. *J. Exp. Biol.* **87**, 65-71.

Mebs, T. and Scherzinger, W. (2000). *Die Eulen Europas.* Stuttgart: Franckh-Kosmos Verlag.

Music, D. and Schneider, J. M. (2008). Elastic properties of amorphous boron suboxide based solids studied using *ab initio* molecular dynamics. *J. Phys. Condens. Matter* **20**, 1-5.

Nachtigall, W. and Rothe, H.-J. (1982). Nachweis eines "clap-and-fling-Mechanismus" bei einer im Windkanal fliegender Haustaube. *J. Ornithol.* **4**, 439-443.

Neuhaus, W., Bretting, H. and Schweizer, B. (1973). Morphologische und funktionelle Untersuchungen über den lautlosen Flug der Eule (*Strix aluco*) im Vergleich zum Flug der Ente (*Anas platyrhynchos*). *Biol. Zent Bl.* **92**, 495-512.

Oliver, W. and Pharr, G. (1992). Measurement of hardness and elastic modulus by instrumented indentation: advances in understanding and refinements to methodology. *J. Mater. Res.* **7**, 1564.

Pannkuk, E. L., Siefferman, L. M. and Butts, J. A. (2010). Colour phases of the eastern screech owl: a comparison of biomechanical variables of body contour feathers. *Funct. Ecol.* **24**, 347-353.

Pennycuik, C. (1968). A wind-tunnel study of gliding flight in the pigeon *Columba livia. J. Exp. Biol.* **49**, 509-526.

Proctor, N. and Lynch, P. (1993). *Manual of Ornithology.* New Haven and London: Yale University Press.

Purslow, P. P. and Vincent, J. F. V. (1978). Mechanical properties of primary feathers from the pigeon. *J. Exp. Biol.* **72**, 251-260.

Rayner, J. M. V. (1993). On aerodynamics and the energetics of vertebrate flapping flight. *Contemp. Math.* **141**, 351-400.

Rüppell, G. (1980). *Vogelflug.* Hamburg: Rowohlt Taschenbuch Verlag.

Stettenheim, R. R. (2000). The integumentary morphology of modern birds – an overview. *Am. Zool.* **40**, 461-477.

Taylor, A. M., Bonser, R. H. C. and Farrent, J. W. (2004). The influence of hydration on the tensile and compressive properties of avian keratinous tissues. *J. Mater. Sci.* **39**, 939-942.

Taylor, I. (1994). *Barn Owls: Predator–Prey Relationships and Conservation.* Cambridge: Cambridge University Press.

Tobalske, B. and Dial, K. (1996). Flight kinematics of black-billed magpies and pigeons over a wide range of speeds. *J. Exp. Biol.* **199**, 263-280.

Usherwood, J., Hedrick, T., McGowan, C. and Biewener, A. (2005). Dynamic pressure maps for wings and tails of pigeons in slow, flapping flight, and their energetic implications. *J. Exp. Biol.* **208**, 355-369.

Weber, T. P., Kranenbarg, S., Hedenström, A., Waarsing, J. H., Weinans, H. (2010). Flight feather shaft structure of two warbler species with different moult schedules: a study using high-resolution X-ray imaging. *J. Zool.* **280**, 163-170.